

This is a repository copy of *Long term phase separation dynamics in liquid crystal-enriched microdroplets obtained from binary fluid mixtures*.

White Rose Research Online URL for this paper:

<https://eprints.whiterose.ac.uk/id/eprint/195098/>

Version: Accepted Version

---

**Article:**

Patel, Mehzabin, Shimizu, Seishi [orcid.org/0000-0002-7853-1683](https://orcid.org/0000-0002-7853-1683), Bates, Martin A. [orcid.org/0000-0003-3482-3577](https://orcid.org/0000-0003-3482-3577) et al. (2 more authors) (2023) Long term phase separation dynamics in liquid crystal-enriched microdroplets obtained from binary fluid mixtures. *Soft Matter*. pp. 1017-1024. ISSN: 1744-683X

<https://doi.org/10.1039/D2SM01348G>

---

**Reuse**

This article is distributed under the terms of the Creative Commons Attribution (CC BY) licence. This licence allows you to distribute, remix, tweak, and build upon the work, even commercially, as long as you credit the authors for the original work. More information and the full terms of the licence here:

<https://creativecommons.org/licenses/>

**Takedown**

If you consider content in White Rose Research Online to be in breach of UK law, please notify us by emailing [eprints@whiterose.ac.uk](mailto:eprints@whiterose.ac.uk) including the URL of the record and the reason for the withdrawal request.

# Soft Matter

Accepted Manuscript

This article can be cited before page numbers have been issued, to do this please use: M. Patel, S. Shimizu, M. Bates, A. Fernandez-Nieves and S. Guldin, *Soft Matter*, 2023, DOI: 10.1039/D2SM01348G.



This is an Accepted Manuscript, which has been through the Royal Society of Chemistry peer review process and has been accepted for publication.

Accepted Manuscripts are published online shortly after acceptance, before technical editing, formatting and proof reading. Using this free service, authors can make their results available to the community, in citable form, before we publish the edited article. We will replace this Accepted Manuscript with the edited and formatted Advance Article as soon as it is available.

You can find more information about Accepted Manuscripts in the [Information for Authors](#).

Please note that technical editing may introduce minor changes to the text and/or graphics, which may alter content. The journal's standard [Terms & Conditions](#) and the [Ethical guidelines](#) still apply. In no event shall the Royal Society of Chemistry be held responsible for any errors or omissions in this Accepted Manuscript or any consequences arising from the use of any information it contains.

Cite this: DOI: 00.0000/xxxxxxxxxx

# Long term phase separation dynamics in liquid crystal-enriched microdroplets obtained from binary fluid mixtures

Mehzabin Patel,<sup>a</sup> Seishi Shimizu,<sup>b</sup> Martin A. Bates,<sup>b</sup> Alberto Fernandez-Nieves,<sup>c,d,e</sup> Stefan Guldin<sup>\*a</sup>Received Date  
Accepted Date

DOI: 00.0000/xxxxxxxxxx

**The dynamics of long term phase separation in binary liquid mixtures remains a subject of fundamental interest. Here, we study a binary liquid mixture, where the minority phase is confined to a liquid crystal (LC)-rich droplet, by investigating the evolution of size, defect and mesogen alignment over time. We track the binary liquid mixture evolving towards equilibrium by visualising the configuration of the liquid crystal droplet through polarisation microscopy. We compare our experimental findings with computational simulations and elucidate differences between bulk and confined droplets based on the respective thermodynamics of phase separation. Our work provides insights on how phase transitions on the microscale can deviate from bulk phase diagrams with relevance to other material systems, such as the liquid–liquid phase separation of polymer and protein solutions.**

## 1 Introduction

Binary fluid mixtures exhibit a miscibility gap for certain compositions and temperature ranges. A phase diagram may present a lower critical solution temperature (LCST) or upper critical solution temperature (UCST). Entering the miscibility curve in the corresponding phase diagram of temperature  $T$  and composition  $x$  induces phase separation either by spinodal decomposition or by nucleation and growth.<sup>1</sup> The dynamics of this liquid–liquid phase separation has been the subject of numerous investigations

in food science, polymer physics and most recently, cell biology.<sup>2</sup> In nucleation and growth processes, the spontaneous formation of nuclei upon cooling of binary fluid systems has been studied from the perspective of a phase ordering process.<sup>3–7</sup> The dynamics in the late stage of the phase separation received considerable attention. In principle, after the initial processes of nucleation and coarsening, domain growth of the new phases proceeds through a sequence of physically distinct hydrodynamic, viscous or inertial effects which ultimately lead to thermodynamic equilibrium.<sup>8–12</sup>

Liquid crystals have been studied as one or both components of a binary liquid mixture. They offer unique characteristics for investigating mesophasic ordering and phase transitions.<sup>13</sup> The surface anchoring of liquid crystal molecules, and unique optical and rheological properties, imply that they are strongly influenced by their local molecular composition.<sup>14,15</sup> This effect is exacerbated when they are under curved confinement due to the introduction of defects. In droplet form they possess large interfacial area, defined director configurations, tunable optical properties and present stimuli response.<sup>16–23</sup> To this end, the effect of confinement on the director configurations and phase transitions of liquid crystals is of interest for the fundamental science of phase transitions, and isotropic-to-nematic phase transitions have been studied experimentally<sup>13,24,25</sup> and theoretically<sup>26–28</sup> over the years.

The effect of nonmesogenic species, in particular polymers, on the phase transitions of liquid crystals is relevant for understanding mesogenic order and tuning viscoelastic properties.<sup>13,29–37</sup> Thoen et al. found solutes such as biphenyl and cyclohexane caused a linear decrease in the nematic-to-isotropic and the nematic-smectic-A transition temperature with increasing mole fraction. The nematic-to-isotropic transition was described as a first-order transition, where the latent heat did not change with mole fraction of the solute.<sup>36</sup> Studies using hexane as a solute, however, found that the isotropic-to-nematic phase transi-

<sup>a</sup> Department of Chemical Engineering, University College London, Torrington Place, London, WC1E 7JE, U.K.; E-mail: s.guldin@ucl.ac.uk <sup>b</sup> Department of Chemistry, University of York, Heslington, York YO10 5DD, United Kingdom <sup>c</sup> Department of Condensed Matter Physics, University of Barcelona, 08028 Barcelona, Spain <sup>d</sup> ICREA-Institució Catalana de Recerca i Estudis Avançats, 08010 Barcelona, Spain <sup>e</sup> Institute for Complex Systems (UBICS), University of Barcelona, 08028 Barcelona, Spain

† Electronic Supplementary Information (ESI) available: [details of any supplementary information available should be included here]. See DOI: 00.0000/00000000.



tion shifts toward lower temperatures nonlinearly with increasing mole fraction.<sup>13</sup> It was deduced that the addition of a solvent diluted the liquid crystal, resulting in an impurity mechanism which introduced a concentration fluctuation and softened the viscoelastic properties of the mixture with respect to that of pure liquid crystal.<sup>13</sup>

Serrano and Fornerod *et al.* investigated a binary liquid mixture of an isotropic liquid, methanol, with liquid crystal 4-Cyano-4'-pentylbiphenyl (5CB).<sup>38</sup> The dilution using methanol reduced and allowed to finely tune the isotropic-to-nematic transition temperature of 5CB.<sup>38,39</sup> Methanol was miscible with 5CB below 10 vol%, but reduced the isotropic-to-nematic phase transition temperature from 35 °C with increasing volume fraction down to 7.8±0.4 °C (at 10 vol% methanol). Above 10 % methanol, the binary mixture displayed an isotropic-isotropic liquid phase separation with decreasing temperature, and an isotropic-to-nematic phase transition of the LC component as the temperature was lowered further. The phase behaviour of 5CB with ethanol as non-nematogenic component was subsequently studied by Reyes *et al.*<sup>40</sup> While the study by Serrano and Fornerod *et al.* provided some indication over non-equilibrium phase separation aspects (see ESI in<sup>38</sup> on isotropic-isotropic coexistence upon cooling), Reyes *et al.* developed a comprehensive picture over non-equilibrium phase separation aspects, in particular related to phase coexistence (isotropic-isotropic, isotropic-nematic) upon cooling and heating. Furthermore, they established a detailed phase diagram of 5CB and ethanol containing both regions of spinodal and binodal decomposition.

Crucially, they found that the isotropic-isotropic phase coexistence within this mixture may be stable above room temperature (in fact, up to ≈ 60 °C) upon the addition of small traces of water (< 5 vol%), which can be used to manipulate structure formation or mixing processes that make use of such of LC-alcohol mixtures.

Building on the above work, a study by Patel *et al.* showed that cooling of an off-critical mixture of a binary fluid composed of liquid crystal 5CB and methanol led to nucleation and growth of liquid crystal-rich droplets, which were found isotropic or nematic depending on the temperature and could be tuned in size and number by temperature quench and cooling rate, respectively.<sup>41</sup>

Herein, we track the evolution of a nematic liquid crystal enriched droplet that is obtained from a binary mixture with methanol. On the one hand, this offers a unique mode for investigating the phase separation of binary liquid mixtures evolving towards equilibrium, as the process can be tracked through changes in the texture of the liquid crystal-rich droplet. On the other hand, our work explicitly addresses whether droplet confinement affects phase equilibria. We address both aspects experimentally using polarised optical microscopy, relying on computer simulations and thermodynamic considerations to rationalize our results and elucidate the role of droplet confinement on the phase behavior.

## 2 Results and discussion

### Experimental results

In a binary liquid mixture of 30% 4-Cyano-4'-pentylbiphenyl (5CB) and 70% MeOH, isotropic 5CB-rich nucleated in the methanol-rich continuous phase upon cooling the mixture below the upper critical solution temperature (UCST) of 22 °C. Further cooling to −1 °C, resulted in an isotropic-to-nematic phase transition of 5CB-rich droplets. The phase diagram for this phenomenon was described by Serrano *et al.*,<sup>38,39</sup> and we have previously investigated droplet formation by this process.<sup>41</sup> The nematic 5CB-rich droplets adopted a radial configuration, with the single point defect at the centre of the droplet as described in Figure 1a.

Prior to isotropic-to-nematic transition of 5CB-rich droplets in the methanol-rich continuous phase, the phase separation of isotropic 5CB-rich droplets was dominated by coalescence. After adopting nematic order, 5CB-rich droplets no longer coalesced, even those in close proximity or even touching. Terentjev explained theoretically that the enhanced stability of nematic emulsions over their isotropic counterparts was due to the energy barrier that needs to be overcome due to the internal mesogen reorganization inside nematic droplets.<sup>42</sup> Therefore, phase separation could only proceed further by other growth mechanisms.

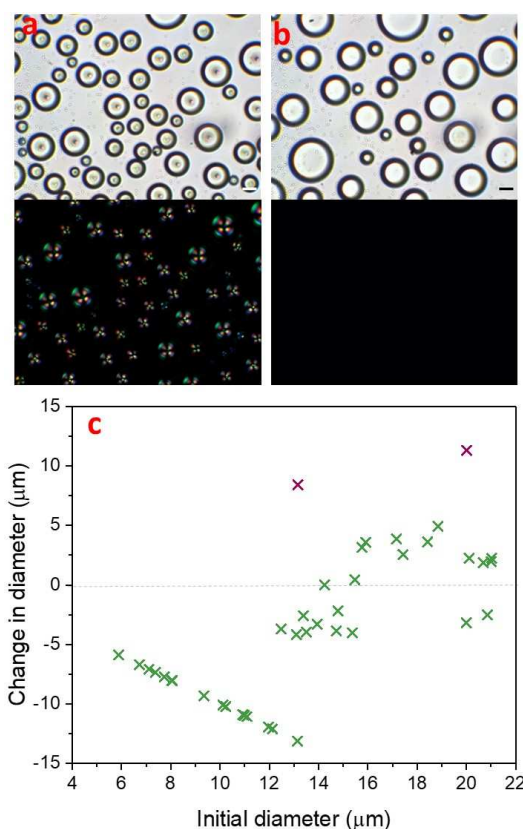


**Fig. 1** Liquid crystal 5CB-rich droplet size progression over time. Bright-field (Top) and cross-polarised (Bottom) images of 5CB-rich droplets (a) after isotropic-to-nematic transition at −5 °C and (b) when turning isotropic again after ≈ 120 minutes at −5 °C. Scale bar: 10 μm. (c) Change in diameter of droplets during nematic lifetime, i.e. between (a) and (b). Note that the data points coloured in purple relate to droplets that had undergone coalescence.





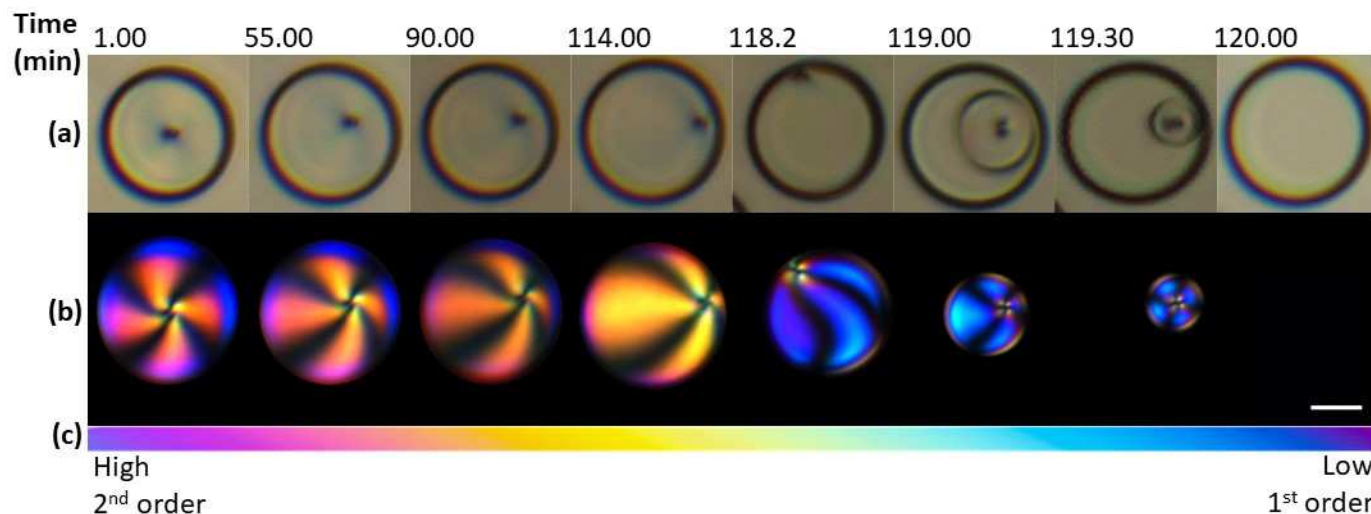


**Fig. 2** Birefringence measurements. Evolution of 5CB-rich droplets under (a) Brightfield (b) crossed polarised light over time. (left–right) (c) Colours of the Michel-Levy chart representing decreasing birefringence. The scale bar represents 10  $\mu\text{m}$  for (a) and (b).

Figure 1(a and b) demonstrates how the partitioning of 5CB-rich droplets evolved during their nematic lifetime, from many smaller droplets ( $13.7 \pm 4.9 \mu\text{m}$ ) immediately after isotropic-to-nematic transition (Figure 1a), to fewer droplets with a larger size distribution ( $19.5 \pm 6.5 \mu\text{m}$ ), 2 hours later when the droplets had lost their nematic order (Figure 1b). With increasing time  $t$ , the small droplets shrank as the solvent diffused through the majority phase into the larger droplets through a process known as Ostwald ripening. Ostwald ripening occurs in order to reduce the total interfacial area of a system via a diffusional mass transfer process from regions of high interfacial curvature to regions of low interfacial curvature. The total interfacial area decreases and larger droplets grow with time in order for the system to reach thermodynamic equilibrium.<sup>43</sup> In an off-critical partially miscible liquid mixture, the amount of each component dissolved in the other is expected to approach the equilibrium state. This amount is determined by the Lever rule.<sup>44,45</sup>

In order to understand the effect of Ostwald ripening in this system, we studied the shrinking and growth of droplets, and analysed their change in diameter and volume over time. Figure 1c highlights the diameter change of each droplet in an image frame (with a green cross) from the isotropic-nematic transition point to 120 minutes later after the nematic-to-isotropic transition. In the frame of the image, the sample size was 40 droplets. The two purple crosses represent droplets whose diameter change was largely related to coalescence. The graph shows many small droplets shrinking and being reabsorbed to increase the volume of fewer larger droplets. The graph shows a linear plot for droplets with diameter  $\leq 13 \mu\text{m}$  which ultimately disappeared completely into the methanol-rich phase. The remaining droplets with a diameter above  $\approx 13 \mu\text{m}$  underwent a change in diameter of up to  $\pm 5 \mu\text{m}$ . Overall, there was a total increase in volume by 15%, which may be attributed an increasing volume of methanol entering the droplet in order to reach equilibrium. In addition to a change in size over time, Figure 1a to b shows a visible deviation of the droplets under cross-polarisation, as the radial point defect

was no longer observed in Figure 1b.

Further, we investigated the evolution of an individual 5CB-rich droplet in the methanol-rich phase at a constant temperature of  $-5^\circ\text{C}$  over time, as shown in Figure 2. The first droplet image, Figure 2a/b–left, was taken at the isotropic-to-nematic transition and the following images were acquired at characteristic intervals until the final image, which was taken after the nematic-to-isotropic transition, i.e. 120 minutes later. In the first 114 minutes, the radial defect in the centre of the LC moved gradually to the surface of the droplet, presenting the droplet in an escaped-radial configuration.<sup>46</sup> After the defect reached the surface of the droplet, the nematic order in the droplet decreased by the formation of an isotropic shell on the outside of the drop, while the centre remained nematic. In the following 2 minutes, this nematic sphere shrunk and eventually disappeared completely, resulting in an entirely isotropic 5CB-rich droplet. While the total time for the evolution of initially nematic droplets back into the isotropic phase deviated by up to 10% between experiments, the observations on defect movement and phase transition were found consistent for all droplets in the field of view, regardless of their size. This is shown in the Supporting Information (SI, Fig. S1).

The way in which the nematic-to-isotropic transition transpired inside the droplet is in contrast to research on a 5CB droplet immersed in silicone oil, where the nematic phase would disappear at several locations inside the droplet before the droplet transitioned to the isotropic phase.<sup>25,47</sup> The radial to escaped-radial movement of a defect has been observed in previous studies during a topological transformation, often induced by an electric field, where a radial droplet transforms from a radial to an axial configuration.<sup>21</sup> Other studies also identified morphological transitions when liquid crystal droplets passed a certain critical threshold radius, e.g. from bipolar, pre-radial to radial ordering with reducing size for planar anchoring.<sup>17,48,49</sup> However, this was typically observed in the sub- $\mu\text{m}$  domain.

We observed the change in nematic order further through the



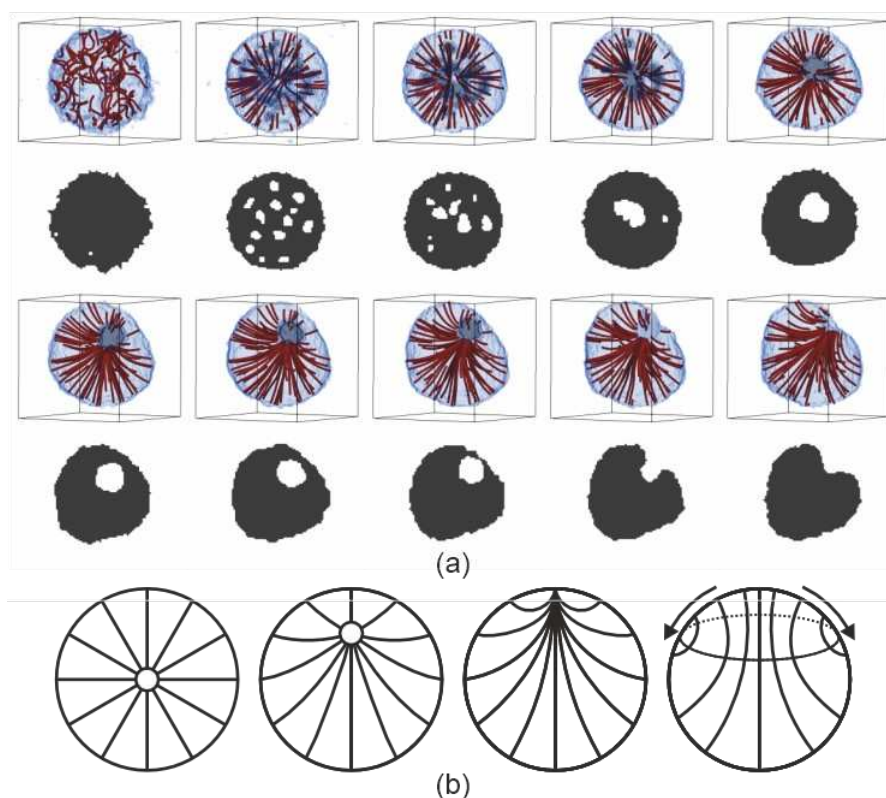


**Fig. 3** Defect formation and progression observed through the simulations. (a) The 3D images show the LC rich regions (blue) and the enclosed LC poor regions (grey) of the droplet. The red streamlines indicate the local orientation within the LC rich region. The 2D images show a planar cut through the droplet at equivalent times, with LC rich regions shown in black. From left to right, top row then bottom row: at time zero, the droplet is quenched from the isotropic and is both orientationally disordered and homogeneous in concentration; as time progresses, the excess solvent near the surface escapes and solvent deep inside the droplet starts to phase separate at the same time as the anchoring at the interface induces a radial configuration; the separation evolves to a single small inner droplet at the core of the radial defect; this droplet and the (virtual) defect in the director field gradually moves towards the surface until it touches the exterior, leaving an escaped radial configuration. (b) Cartoon of the evolution of the director configuration from radial to escaped radial as the inner droplet moves from the centre to the surface of the droplet. After expulsion, the escaped radial either remains or transforms to axial, as shown.

decreasing retardation over time. Comparing the colours of the droplets to those on a Michel-Levy chart, Figure 2c, the decreasing birefringence over time is evident, with the polarisation going from second to first order colours. Additionally, within each droplet, the order of interference colours seen in the isochromes decreased towards the melatope.

The occurrence of thermal gradients as a possible cause of the observed effect was investigated via thermal imaging of the sample and the surrounding area (Supplementary Information, Fig. S2). The results demonstrate that the temperature of the stage remained constant at least  $2^{\circ}\text{C}$  below the nematic-isotropic temperature over the full period of investigation (90 min).

### Computer simulations

We deployed computer simulations to gain further insight into the formation and progression of the defect arrangement within a single two component droplet. We used a simple coarse grained model (see SI) to represent small volumes of the two components and tailored the interactions between these volumes to reproduce a phase diagram that is qualitatively similar to the experimental one and also presents homeotropic anchoring at the droplet surface.

A small spherical droplet was prepared with the appropriate compositions of the minority and majority phases from the bulk phase diagram and equilibrated at a temperature just above the (bulk) transition to the nematic phase. The evolution of the small model droplet is shown in Fig. 3. On cooling the isotropic droplet into the nematic phase, the homeotropic surface anchoring rapidly induces a radial defect at the centre of the droplet. Due to the temperature change, and unlike pure LC droplets, the composition of the binary mixture droplet is no longer in equilibrium and the minority phase inside the droplet has an excess of solvent. Solvent near the surface of the droplet can easily escape to the surrounding majority phase. Similarly, excess LC in the minority phase can be absorbed into the droplet. However, the excess solvent within the droplet but far enough away from the outer interface was observed to phase separate within the droplet forming many small methanol-rich droplets. To minimise the elastic energy of the nematic droplet, these internal phase separated methanol droplets either leave the droplet (if near the surface) or congregate near the radial defect observed in the director field; the high splay energy point defect is partially stabilised by becoming a virtual point defect within an inner droplet formed of excess solvent. As time progresses, both the virtual defect and

the interior methanol droplet slowly move towards the surface. As the interior solvent-rich droplet reaches the exterior majority phase, this pins a now escaped-radial defect at the surface of the droplet. Once the defect has reached the surface, two different types of behaviour can be observed. If quenched at lower temperatures, the escaped radial defect tends to remain at the surface and appears to be stable. At higher temperatures, the director configuration transforms from escaped radial into an axial configuration (as shown in the SI). In these simulations we do not observe the shrinking of the nematic region of the droplet as in the experiments. Of course, there are a number of assumptions that are necessarily made that could be responsible for differences between the experimental and simulated systems once the defect reaches the surface.

To be computationally tractable, we assume that each droplet can be investigated as a single small isolated system once the temperature is dropped. A relatively large temperature jump between the isotropic and nematic phase was used to examine the behaviour when the composition is out of equilibrium to be sure to identify changes in homogeneity in composition. However, a similar time dependent behaviour of the director field is observed when using a smaller temperature difference either side of the phase transition, but the formation of an internal droplet in this case is less clear since the compositions of the two phases are much closer to each other. It is also necessary to make assumptions about the relative balance of the potential for nematic ordering compared to that of surface anchoring and that of immiscibility between the two components. The values chosen give a qualitatively realistic bulk phase diagram and lead to homeotropic anchoring at an interface. The observation that the director field can change from escaped radial to axial is likely due to the surface anchoring being large compared to the bend bulk elastic constant combined with the small droplet size and hence the large surface to volume ratio.

It may also be that small deviations in the parameters could change the longer time behaviour once the radial defect reaches the surface of the droplet, especially if the slow influx of individual methanol molecules across the interface, which is not accounted for in the coarse grained model, is responsible for the diminishing order at the surface. In both experiment and simulation, it is apparent that the size of the nematic region is reasonably constant while the defect core remains inside the droplet and the formation and motion of the defect in the simulations appears similar to that in the experiment. The observed behaviour deviates only once the defect reaches the surface. We can therefore speculate that the existence of a region of disorder at the interface is responsible for the subsequent shrinkage of the nematic region. Since the defect represents a region of disorder, the composition within the defect region is likely to be different to that of the bulk majority and minority phases. This imperfection at the surface may allow methanol from the surrounding environment to enter the nematic region, causing the region around the defect to transform to the isotropic (minority) phase, with the droplet size remaining constant but the nematic region shrinking, while retaining the escaped radial defect at the interface between the nematic and isotropic regions of the droplet.

Simulations of the model also allow us to run a control experiment not possible with the real droplets, where the starting isotropic droplet has the (bulk) composition of the final, lower temperature nematic phase. In this case, there should be no excess solvent inside the droplet when cooled. When simulations are run at this composition, the droplet is observed to either initially start to form a radial structure due to the surface anchoring, which rapidly transforms to axial as a central bulk-like nematic region grows, or, more frequently, the axial configuration forms directly on cooling. Therefore it seems likely that the presence of excess solvent inside the defect on cooling from the isotropic is responsible for inhomogeneity in composition within the droplet and helps to stabilise the overall radial director structure of the droplet by removing the highly strained splay defect region.

## Discussion

Depending on the mixing composition, a binary mixture of 5CB and methanol may phase separate; the mixture composition of each phase is determined by the phase diagram and the relative phase amounts can be evaluated by the Lever rule.<sup>44,45,50</sup> For example, in a 70:30 vol%:vol% MeOH:5CB mixture, the methanol-rich phase is composed of 76.6 vol% MeOH and 23.4 vol% 5CB at  $-5^{\circ}\text{C}$  and in equilibrium, and the LC-rich minority phase is composed of 88.5 vol% 5CB and 11.5 vol% MeOH. The changing internal configuration of the LC-rich droplet described in Figure 2 may be attributable to the shift in equilibrium of the binary mixture that accompanies the uptake of methanol in the 5CB-rich droplet; we will discuss this below. In return, this uptake of methanol may cause a deformation of the director due to the changing elastic energy of the LC, as explained by Sigdel and De-nolf.<sup>13,36</sup>

Thus, we have observed a loss of nematic order in the droplet over time, which we relate to an uptake of methanol. Such an observation could be supported by the drop size effect on the thermodynamics of phase equilibria. We note that a regular phase diagram will account for phase separation and nematic-to-isotropic phase transition in the bulk phase. However, the results found in micro-scale phase separation exhibited a deviation from the bulk phase diagram. Consequently, we must clarify thermodynamically how the droplet size affects the nematic-to-isotropic phase boundary. Such a setup of the problem is consistent with our experiment (Figure 2) and simulation (Figure 3), in which we addressed how an unstable nematic droplet turns into an isotropic droplet. At the nematic-isotropic phase boundary, the chemical potentials of both components in the two phases are equal. Our goal is to clarify how this phase boundary is affected by the droplet size, composition, and temperature. The context of the problem invokes more degrees of freedom than are allowed from the standard Gibbs phase rule: a 2-component system forming 3 phases (the nematic droplet phase, the isotropic droplet phase, and the bulk isotropic phase that surrounds the droplet) has  $F = 2 - 3 + 2 = 1$  degree of freedom. Hence, keeping the pressure constant would leave no degree of freedom. However, unlike an isotropic macroscopic system, the experimental microscopical system presented herein may present additional degrees





of freedom. One is “the number of independent length scales influencing the free energy”<sup>3</sup> that characterises the difference between the nematic and isotropic phases; the droplet radius  $R$  in our case.<sup>1–3</sup> Furthermore an additional degree of freedom is related to the boundary effect in microscopic systems,<sup>4</sup> since the interfacial tension that cannot be neglected for small  $R$ . The problem is formulated in the Supplementary Information as a deviation from the bulk phase diagram, corresponding to  $R^{-1} = 0$ . The chemical potentials in the droplet are expressed as  $\mu_s^{(i)}$ ,  $\mu_m^{(i)}$ ,  $\mu_s^{(n)}$ , and  $\mu_m^{(n)}$  for 5CB and methanol in isotropic (denoted with the superscript  $(i)$ ), and nematic (denoted with the superscript  $(n)$ ) phases, respectively. Based on thermodynamic arguments (SI), how methanol mole fraction at the nematic-isotropic phase boundary  $x_m$  shifts ( $\delta x_m$ ) with the change in droplet size  $\delta R^{-1}$  can be expressed as:

$$\frac{\delta x_m}{\delta R^{-1}} = - \frac{\left( \frac{\partial \Delta \mu_\alpha}{\partial R^{-1}} \right)_{T, x_m}}{\left( \frac{\partial \Delta \mu_\alpha}{\partial x_m} \right)_{T, R^{-1}}} \quad (1)$$

where  $\Delta \mu_\alpha$  is the chemical potential difference of  $\alpha$  ( $=m$  for methanol or  $=s$  for 5CB) between the nematic and isotropic phases (i.e., nematic minus isotropic).

We now apply equation 1 to understand the droplet effect on nematic stability. We observed the disappearance of the nematic phase in droplets, even though at the same (mole fraction of methanol ( $x_m$ ), temperature ( $T$ )) the bulk nematic phase was observed to be stable. This suggests a decrease in nematic phase stability, or equivalently a shift of nematic-to-isotropic boundary towards lower  $x_m$  as  $R^{-1}$  increases, leading to  $\frac{\delta x_m}{\delta R^{-1}} < 0$ . Assuming that  $\left( \frac{\partial \Delta \mu_s}{\partial x_m} \right)_{T, R^{-1}} > 0$  still holds true for droplets, we obtain  $\left( \frac{\partial \Delta \mu_s}{\partial R^{-1}} \right)_{T, x_m} > 0$ . This means that the relative stability of 5CB in the nematic phase decreases as the droplet becomes smaller. For methanol in droplets, assuming that  $\left( \frac{\partial \Delta \mu_m}{\partial x_m} \right)_{T, R^{-1}} < 0$  still holds true for a deviation from the bulk ( $R^{-1} = 0$ ) (see Supplementary Information (SI) for details), we obtain  $\left( \frac{\partial \Delta \mu_m}{\partial R^{-1}} \right)_{T, x_m} < 0$ . As a result, the relative stability of methanol in the nematic phase increases as the droplet becomes smaller. Thus, the nematic phase is made less stable in smaller droplets by the destabilisation of 5CB and stabilisation of methanol, consistent with our findings from simulation.

Furthermore, in a binary liquid mixture with partial miscibility, there is a diffuse interface barrier between the phases, which is defined by interfacial tension, and increases with temperature.<sup>3,39</sup> Here, the diffuse interface barrier between the 5CB-rich phase and methanol-rich phase allowed exchange of individual molecules between the two components, and therefore the amount of methanol in the 5CB-rich phase increased in order to eventually reach the equilibrium state. At equilibrium, there is no chemical potential difference across the phase boundary, and thus no net diffusive flux.<sup>51</sup> In a similar manner, the increasing amount of an isotropic liquid in a liquid crystal droplet has been described in a study by Denolf and Sigdel as a dilution effect.<sup>13,36</sup> The addition of a solvent to a liquid crystal influenced

the isotropic-to-nematic transition and resulted in softening of the viscoelastic properties of the liquid crystal. Therefore, the change in nematic configuration and birefringence can be attributed to the uptake of methanol in the 5CB-rich droplet as it reached equilibrium, which caused a deformation of the director due to the changing elastic energy of the liquid crystal.

We note that after the nematic-to-isotropic transition of the 5CB-rich droplet, the temperature of the system was decreased further from  $-5^\circ\text{C}$  to  $-10^\circ\text{C}$ . With this cooling, the droplets transitioned back to the nematic phase. Thus, a change in temperature caused a shift in the equilibrium conditions. The system worked again towards reaching equilibrium.

### 3 Conclusion

We have shown how the phase behaviour for a binary liquid mixture can deviate from the bulk for small droplets when interfacial tension is introduced. In a binary liquid mixture containing a LC-rich droplet phase at  $-5^\circ\text{C}$ , the internal configuration changed over time resulting in observable differences in the optical properties of the droplet. Droplets transformed from a nematic radial to an escaped-radial configuration and finally a nematic-to-isotropic transition took place after  $\approx 2$  hours. In contrast, the bulk system remained nematic at  $-5^\circ\text{C}$  indefinitely. The experimental evidence for defect formation and motion is further supported through simulations. Crucially, further lowering of the system temperature re-introduced an isotropic-to-nematic transition of the droplets, reinforcing the explanation that methanol uptake is responsible for the nematic-to-isotropic droplet phase transition. Our approach may have ramifications beyond liquid crystals in a generalised context of confinement-induced changes in phase stability,<sup>52</sup> which ranges from small molecules (e.g., ethanol-water mixtures<sup>53–57</sup>) to biomolecular solutions<sup>58–60</sup> and polymer blends,<sup>61</sup> and also in crystallization of proteins in droplets.<sup>62,63</sup>

### Experimental section

**Reagents** The liquid crystal 4-Cyano-4'-pentylbiphenyl (5CB) was obtained from Synthon Chemicals (99.5% (GC)). Methanol (HPLC grade) was purchased from Sigma Aldrich. All compounds were used without further purification.

**Sample preparation** 5CB and methanol were mixed in a glass cuvette, which was enclosed by a Peltier-regulated sample compartment that allowed control over both temperature and stirring (Quantum Northwest, Qpod 2e). Unless stated otherwise, a 30:70 volume ratio of 5CB/RM257:MeOH was used for all experiments. Samples were heated to  $35^\circ\text{C}$  in the cuvette.

**Sample analysis** For microscopic analysis,  $10\ \mu\text{l}$  of the homogeneous 5CB:MeOH mixture was deposited between a glass slide and cover slip and sealed with varnish (purchased from Rimmel: 15-40% ethyl acetate, 15-40% butyl acetate, 5-15% nitrocellulose, 1-10% isopropylalcohol) to prevent methanol evaporation.

The slide was placed under an upright microscope (Zeiss, Axio Scope A1), that was operated in transmission and primarily in brightfield mode. Crossed polarisers were used to observe anisotropic behaviour. A temperature controlled sample stage (Linkam, LTS120) was used for all experiments. Nitrogen was introduced into the chamber to prevent condensation at low tem-





peratures. In situ droplet growth was recorded by time-resolved digital image acquisition using a Lumenera Infinity 3-3UR camera with a resolution of 1936 X 1456 pixels.

The sample stage was pre-heated to 35°C, and then cooled at 20°Cmin<sup>-1</sup> to -5°C. Quantitative droplet investigation was carried out by a bespoke computational image analysis code developed in Python. Droplets from the images were distinguished, and the number of droplets, the average diameter and standard deviation computed as a function of time.<sup>64</sup> Calculation of volumes was carried out using Fiji.

Conflicts of interest

There are no conflicts to declare.

Acknowledgements

MP acknowledges funding as part of the EPSRC Centre for Doctoral Training in Molecular Modelling and Materials Science (EP/L015862/1) in support of BASF SE. AFN is grateful for support by MCIN/AEI/10.13039/501100011033/FEDER, 289 (Grant No. PID2021-122369NB-I00).

Notes and references

1 J. M. Gunton, M. San Miguel and P. S. Sahni, in *Phase Transit. Crit. Phenom.*, ed. J. L. Lebowitz, Academic, London, Vol. 8 edn., 1983, p. 267.

2 C. D. Keating and R. V. Pappu, *J. Phys. Chem. B*, 2021, **125**, 12399–12400.

3 J. W. Cahn and J. E. Hilliard, *J. Chem. Phys.*, 1959, **31**, 688–699.

4 J. W. Gibbs, *The Scientific Papers of J. Willard Gibbs*, Vol. 1, Dover, New York, 1961.

5 H. Reiss and M. Shugard, *J. Chem. Phys.*, 1976, **65**, 5280.

6 A. J. Bray, *Phys. A Stat. Mech. its Appl.*, 1993, **194**, 41–52.

7 J. Colombani and J. Bert, *J. Non-Equilib. Thermodyn.*, 2004, **29**, 389–395.

8 V. S. Nikolayev, D. Beysens and P. Guenoun, *Phys. Rev. Lett.*, 1996, **76**, 3144–3147.

9 J. H. Yao, K. R. Elder, H. Guo and M. Grant, *Phys. A Stat. Mech. its Appl.*, 1994, **204**, 770–788.

10 F. Cau and S. Lacelle, *Phys. Rev. E*, 1993, **47**, 1429–1432.

11 T. Kalwarczyk, N. Ziebac, M. Fiałkowski and R. Holyst, *Langmuir*, 2008, **24**, 6433–6440.

12 R. Limary and P. F. Green, *Langmuir*, 2003, **19**, 2419–2424.

13 K. P. Sigdel and G. S. Iannacchione, *J. Chem. Phys.*, 2010, **133**, year.

14 P. S. Drzaic, *J. Appl. Phys.*, 1986, **60**, 2142–2148.

15 P. S. Drzaic, *Liquid Crystal Dispersions*, World Scientific, 1995.

16 G. P. Crawford and S. Zumer, *Liquid Crystals In Complex Geometries: Formed by Polymer And Porous Networks*, CRC Press, 1996.

17 J. Gupta, S. Sivakumar, F. Caruso and N. Abbott, *Angewandte Chemie International Edition*, 2009, **48**, 1652–1655.

18 M. I. Kinsinger, M. E. Buck, N. L. Abbott and D. M. Lynn, *Langmuir*, 2010, **26**, 10234–10242.

19 W. Khan, J. H. Choi, G. M. Kim and S. Y. Park, *Lab Chip*, 2011, **11**, 3493–3498.

20 I. Lin, D. S. Miller, P. J. Bertics, C. J. Murphy, J. J. D. Pablo and N. L. Abbott, *Science (80-. )*, 2011, **332**, 1297–1300.

21 T. Lopez-Leon and A. Fernandez-Nieves, *Colloid Polym. Sci.*, 2011, **289**, 345–359.

22 A. Concellón, C. A. Zentner and T. M. Swager, *J. Am. Chem. Soc.*, 2019, **141**, 18246–18255.

23 W. S. Wei, Y. Xia, S. Ettinger, S. Yang and A. G. Yodh, *Nature*, 2019, **576**, 433–436.

24 S. Bronnikov, V. Cozan and A. Nasonov, *Phase Transitions*, 2007, **80**, 831–839.

25 X. Chen, B. D. Hamlington and A. Q. Shen, *Langmuir*, 2008, **24**, 541–546.

26 A. Bhattacharya, M. Rao and A. Chakrabarti, *Phys. Rev. E - Stat. Physics, Plasmas, Fluids, Relat. Interdiscip. Top.*, 1996, **53**, 4899–4903.

27 A. J. Bray, *Adv. Phys.*, 2002, **51**, 481–587.

28 Z. Kutnjak, S. Kralj, G. Lahajnar and S. Žumer, *Phys. Rev. E - Stat. Physics, Plasmas, Fluids, Relat. Interdiscip. Top.*, 2003, **68**, 12.

29 R. L. Humphries and G. R. Luckhurst, *Proc R Soc London Ser A*, 1976, **352**, 41–56.

30 M. Mucha, *Prog. Polym. Sci.*, 2003, **28**, 837–873.

31 E. R. Soule and A. D. Rey, *Mol. Simul.*, 2012, **38**, 735–750.

32 R. Shimada and H. Watanabe, *J. Soc. Rheol., Jpn*, 2020, **48**, 199–206.

33 R. Shimada, O. Urakawa, T. Inoue and H. Watanabe, *Soft Matter*, 2021, **17**, 6259–6272.

34 P. K. Mukherjee, *J. Chem. Phys.*, 2002, **116**, 9531–9536.

35 S. DasGupta and S. K. Roy, *Phys. Lett. Sect. A Gen. At. Solid State Phys.*, 2001, **288**, 323–328.

36 K. Denolf, G. Cordoyiannis, C. Glorieux and J. Thoen, *Phys. Rev. E - Stat. Nonlinear; Soft Matter Phys.*, 2007, **76**, 1–9.

37 S. Thakur, P. A. Pullarkat and P. B. Kumar, *Phys. Rev. E - Stat. Nonlinear; Soft Matter Phys.*, 2009, **80**, 1–7.

38 L. A. Serrano, M. J. Fornerod, Y. Yang, F. Stellacci and S. Guldin, *Soft Matter*, 2018, **14**, 4615–4620.

39 M. J. Fornerod, E. Amstad and S. Guldin, *Mol. Syst. Des. Eng.*, 2020, **5**, 358–365.

40 C. G. Reyes, J. Baller, T. Araki and J. P. F. Lagerwall, *Soft Matter*, 2019, **15**, 6044–6054.

41 M. Patel, A. N. Pallipurath Radhakrishnan, L. Bescher, E. Hunter-Sellars, B. Schmidt-Hansberg, E. Amstad, S. Ibsen and S. Guldin, *Soft Matter*, 2021, **17**, 947–954.

42 E. M. Terentjev, *Europhys. Lett.*, 1995, **32**, 607–612.

43 P.W. Voorhees, *Annu. Rev. Mater. Sci.*, 1992, **22**, 197–215.

44 D. A. Porter and K. E. Easterling, *Phase Transformations in Metals and Alloys*, 1992, pp. 1–227.

45 J. P. Erikson, *J. Chem. Educ.*, 2017, **94**, 75–78.

46 O. O. Prishchepa, V. Y. Zyryanov, A. P. Gardymova and V. F. Shabanov, *Mol. Cryst. Liq. Cryst.*, 2008, **489**, 84–93.

47 Z. Bradač, S. Kralj and S. Žumer, *Phys. Rev. E - Stat. Physics, Plasmas, Fluids, Relat. Interdiscip. Top.*, 2002, **65**, 1–10.

48 V. Tomar, S. I. HernÁndez, N. L. Abbott, J. P. HernÁndez-Ortiz and J. J. de Pablo, *Soft Matter*, 2012, **8**, 8679–8689.

49 Z. Sumer and A. Striolo, *Soft Matter*, 2019, **15**, 3914–3922.

50 S. Puri, *Phase Transitions*, 2004, **77**, 407–431.

51 S. Mehta and J. Zhang, *Nat. Rev. Cancer*, 2022.

52 S. Shimizu and N. Matubayasi, *Phys. A Stat. Mech. its Appl.*, 2021, **563**, 125385.

53 A. Phan, D. R. Cole and A. Striolo, *Langmuir*, 2014, **30**, 8066–8077.

54 C.-H. Wang, P. Bai, J. I. Siepmann and A. E. Clark, *J. Phys. Chem. C*, 2014, **118**, 19723–19732.

55 X.-Y. Guo, T. Watermann and D. Sebastiani, *J. Phys. Chem. B*, 2014, **118**, 10207–10213.

56 M. Zhao and X. Yang, *J. Phys. Chem. C*, 2015, **119**, 21664–21673.

57 T. Muthulakshmi, D. Dutta, P. Maheshwari and P. K. Pujari, *J. Condens. Matter Phys.*, 2018, **30**, year.

58 L. Gelb, K. Gubbins, R. Radhakrishnan and M. Sliwinski-Bartkowiak, *Rep. Prog. Phys.*, 1999, **62**, 1573–1659.

59 Z. Fetahaj, L. Ostermeier, H. Cinar, R. Oliva and R. Winter, *J. Am. Chem. Soc.*, 2021, **143**, 5247–5259.

60 A. Villosio, U. Capasso Palmiero, P. Mathur, G. Perone, T. Schneider, L. Li, M. Salvalaglio, A. deMello, S. Stavakis and P. Arosio, *Small*, 2022, e2202606.

61 R. Cherrabi, A. Saout-Elhach, M. Benhamou and M. Daoud, *J. Chem. Phys.*, 1999, **111**, 8174–8181.

62 S.-M. Yang, D. Zhang, W. Chen and S.-C. Chen, *Lab Chip*, 2015, **15**, 2680–2687.

63 F. Chen, G. Du, D. Yin, R. Yin, H. Zhang, W. Zhang and S.-M. Yang, *Advances In Materials, Machinery, Electronics I*, 2017.

64 A. N. Radhakrishnan, M. P. Marques, M. J. Davies, B. O'Sullivan, D. G. Bracewell and N. Szita, *Lab Chip*, 2018, **18**, 585–594.